Available online at www.sciencedirect.com
SCIENCE DIRECT®
Sensors and Actuators B 107 (2005) 233–241
SENSORS AND ACTUATORS B CHEMICAL
www.elsevier.com/locate/snb

A differential microcantilever-based system for measuring surface stress changes induced by electrochemical reactions

Vincent Tabard-Cossa*, Michel Godin, L.Y. Beaulieu[1], Peter Grütter

Physics Department, McGill University, Rutherford Bldg., 3600 University St., Montréal, Que., Canada

Received 18 May 2004; received in revised form 13 October 2004; accepted 19 October 2004
Available online 28 November 2004

Abstract

We report on a differential microcantilever-based system capable of measuring surface stress changes which occur during electrochemical reactions. Surface stress changes induced by sub-monolayer ionic adsorption on metal surfaces and/or by electromechanical transformations in thin films can be measured. Our system is composed of two microcantilever sensors. The first *active* microcantilever serves as the working electrode (in a conventional three-probe electrochemical cell configuration) and as the mechanical transducer (bending of the microcantilever), yielding simultaneous, real-time, in situ measurements of the current and interfacial stress changes. The second *reference* microcantilever serves as a reference sensor to detect any unwanted cantilever deflection resulting from temperature variations, mechanical vibrations and/or uncontrolled chemical reactions. A technique for isolating the electrical contact made to the microcantilever from the electrolyte solution is presented. A method for creating a working electrode with a reproducible area of 1.0 mm^2 is also described. This micromechanical cantilever sensor has a deflection sensitivity of 0.2 nm, which translates to a surface stress sensitivity of 1×10^{-4} N/m with a dynamic range of 5×10^5. The differential mode of this system has been characterized by measuring the potential-induced surface stress, at the Au(1 1 1) solid–liquid ($HClO_4$ electrolyte) interface, during anion (ClO_4^-) adsorption on gold, while varying the solution temperature. Furthermore, we have measured the surface stress induced during ion doping/dedoping of dodecyl benzenesulfonate-doped polypyrrole (PPy(DBS)) films in an aqueous solution of Na(DBS).

Keywords: Microcantilever sensor; Surface stress; Electrochemistry; Solid–liquid interfaces; Polypyrrole

1. Introduction

Micromechanical devices, based on commercially available atomic force microscopy (AFM) microcantilevers, have the potential to transduce a variety of chemical and physical phenomena into a mechanical movement on the nanometer scale [1]. The major appeal of these microcantilever-based sensors is their versatility. Through an appropriate organic or metallic coating of their surface, they have been shown to transduce a variety of processes involving an applied force, heat, stress, magnetism, charge, radiation, and chemical reactions into a measurable mechanical movement. Moreover, because of their small size (micrometers), these microcantilevers have a short response time (less than milliseconds) and a typical sensitivity at the nanogram (10^{-9}), picoliter (10^{-12}), femtojoule (10^{-15}) and attomolar (10^{-18}) level [2].

Microcantilever-based sensors can be used in *static* mode where a deflection of the free end of a microcantilever, induced by a change in the surface stress of one of its sides, is measured [3]. The interpretation of the origin of the measured surface stress is not trivial based on the microcantilever response alone. For this reason, it can be advantageous to combine this type of sensor with other measurement techniques. Such an approach has been used by Godin et al. [4], who have integrated in situ a microcantilever-based sensor with an ellipsometer and combined it with ex situ STM measurements,

* Corresponding author. Tel.: +1 51 43 988 281; fax: +1 51 43 988 434.
E-mail address: vtabar@physics.mcgill.ca (V. Tabard-Cossa).
[1] Present address: Memorial University, St. John's, NF, Canada A1B 3X7.

0925-4005/$ – see front matter © 2004 Elsevier B.V. All rights reserved.
doi:10.1016/j.snb.2004.10.007

to correlate surface stress, thickness and phase changes occurring during alkanethiol adsorption on gold. Others have combined microcantilever-based sensors with electrochemical techniques by using the micromechanical cantilever sensor as the working electrode (WE), yielding simultaneous, in situ measurements of current (or charge) and surface stress changes. Combining electrochemistry with microcantilever-based sensing allows for kinetics measurements to be performed, and often the ability to study processes occurring on the microcantilever in a reversible fashion. To date, underpotential metal deposition [5–7], electrocapillary-type effects [6–10], doping/dedoping of a conducting polymer film [11,12], and redox reactions at a monomolecular organic film interface [13], have been investigated.

Unfortunately, most of microcantilever sensor results suffer from reproducibility issues. Some results are even contradictory with other bending beam measurements techniques. Indeed, Ibach et al. [14] and Haiss et al. [15] have reported, on well-defined single crystal gold surfaces, a different surface stress response, at the solid–liquid interface, from microcantilever-based sensors. In a recent study, it was clearly shown that the substrate morphology plays a vital role in the response of microcantilever chemical sensors [16]. These experiments underline the fact that up to now the role played by the morphology of the sensing substrate in microcantilever surface stress sensors has been undervalued. Parameters such as adhesion (i.e. adequately transferring the surface stress in the sensing film to the substrate), surface morphology (grain size, roughness, crystallographic orientation) and cleanliness of the metal film can have both qualitative and quantitative effects on the measured surface stress. It is therefore essential to characterize and study these effects on the sensor response if the origin of surface stress is to be understood and if microcantilever-based sensors are to become a useful sensing technology.

In this paper we will describe a complete electrochemical microcantilever-based sensor instrument. Although other groups have used electrochemical microcantilever sensors, none have openly addressed the specific requirements for conducting these types of measurements. In Section 2.2, we will provide a complete description of the integration of a differential micromechanical cantilever-based sensor with a standard three-probe electrochemical system. In particular, in Section 2.2.2, we present a fast, easy, and clean approach to isolate the active microcantilever electrical contact point from the electrolyte solution. Moreover, in Section 2.2.3, we implement a method for reproducibly defining a 1.0 mm^2 working electrode area, which allows for a quantitative measure of the current density, and therefore knowledge of the charge consumed per unit area. In Section 2.3 we discuss the calibration of the surface stress measurements. For the purpose of subtracting any unwanted deflections from the active microcantilever signal, differential surface stress capability was realized in this system and is described in Section 3.1. The differential mode was characterized by varying the cell electrolyte solution temperature while an electrochemical reaction (anion adsorption of ClO_4^-) is being performed on the gold-coated side of the active microcantilever. Lastly, in Section 3.2, the instrument was tested by studying the doping/dedoping of dodecyl benzenesulfonate-doped polypyrrole (PPy(DBS)) films in an aqueous solution of Na(DBS), showing the bending response of the PPy/Au-coated microcantilever as a function of the applied potential, simultaneously yielding real-time, in situ, electrochemical and surface stress information.

2. Experimental

2.1. Materials and methods

All experiments were performed in the electrochemical cell described in Section 2.2. The cell was machined from a chemically inert material, Teflon®. The cell is equipped with a 3 M NaCl Ag/AgCl reference electrode (model RE-6) from BioAnalytical Systems (USA) and a 2 cm long, 1 mm diameter, 99.99% purity, platinum wire from Alpha Aesar (USA) as a counter electrode, connected to a BioAnalytical Systems 50CW potentiostat. Prior to each experiment, the cell is rinsed three times with high purity de-ionized water (Millipore Simplicity 185 water system), followed by the electrolyte solution. The pyrrole monomer liquid (Aldrich, Canada) is purified by passage through an alumina-filled column. The resulting liquid is clear and colorless in appearance, indicating that the long pyrrole chains, from spontaneous polymerization, are removed. The aqueous solution containing pyrrole and NaDBS (Aldrich, Canada) is purged with argon gas and protected from ambient light following its preparation to prevent polymerization of the monomer.

The microcantilever sensors used herein are rectangular silicon cantilevers from MikroMasch (Estonia) type CSC12/without Al/tipless, with a typical length, width, thickness, and spring constant of 350 μm, 35 μm, 1 μm, and 0.03 N/m, respectively. However, these dimensions were independently measured for each microcantilever used to improve on the accuracy of the measured surface stress as described in Section 2.3. The surface of the silicon microcantilevers was coated with 100 nm of gold (99.99%, Plasma Materials, USA) on a 10 nm titanium (99.99%, Alfa Aesar, USA) adhesion layer with a thermal evaporator (model VE90, Thermionics Laboratories, USA). The evaporation was conducted under a pressure below 5.0×10^{-6} Torr, at a rate of 0.14 nm/s for Au, and 0.04 nm/s for Ti. Radiative heating of the evaporation boat increased the microcantilevers temperature to $130 \pm 20\,^{\circ}C$.

2.2. Description of the combined instrument

Fig. 1 shows a schematic representation of the differential microcantilever-based sensor combined with a standard three-electrode system composed of an Ag/AgCl reference

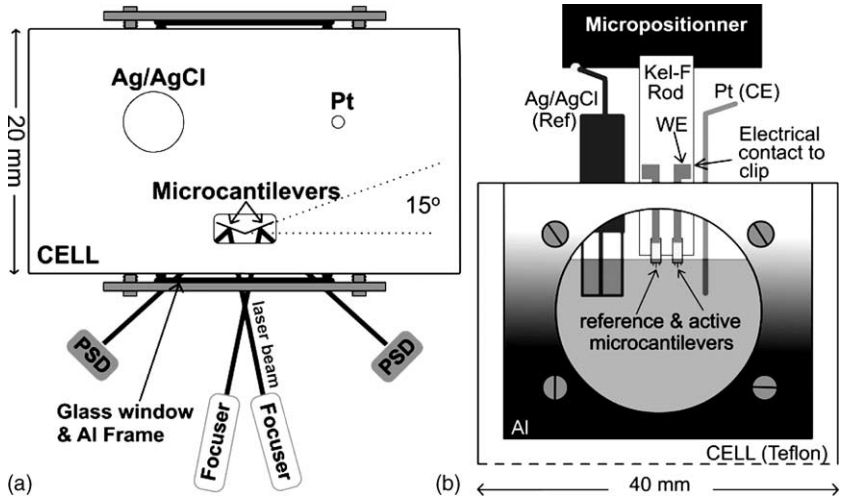

Fig. 1. (a) Top view of the system. The laser light passes through a glass window and is reflected off the microcantilever before reaching the PSD. The three electrodes present in the cell form an equilateral triangle. A schematic representation of the front of the cell is shown in (b). The vertically mounted microcantilever chip is immersed into the electrolyte solution using a micropositioner. On the Kel-F rod, the microcantilever chip is mechanically held by a metal clip with which electrical contact is made. The Kel-F rod can be flipped in order to reflect the laser beam on either side of the microcantilevers.

electrode (RE), and a platinum wire as a counter electrode (CE). A gold-coated, rectangular-shaped, tipless, silicon microcantilever is used as the active microcantilever, serving as both the working electrode (WE) and as the sensing platform of the surface stress sensor. A second identical gold-coated microcantilever is used as a reference sensor. A commercial potentiostat is used to apply a potential to the active microcantilever (WE) and to monitor the current response during cyclic voltammetric experiments. In parallel, an optical beam technique is used to monitor the microcantilevers' deflections.

2.2.1. The cell

The cell was designed to accommodate the constraints imposed by the electrochemical and the microcantilever sensor experiments. The electrochemical aspect of the combined instrument requires three electrodes, RE, CE and WE. The WE is the platform on which the electrochemical reaction takes place. This electrochemical reaction can result in organic or metal thin film deposition, ion adsorption or produce any types of redox reactions on the WE surface, etc. This reaction is compensated at the CE. Current flows between the WE and CE. The presence of the RE provides an equilibrium reaction that determines the reference level in the electrochemical cell. No current flows through the RE. The CE area is about 100 times larger then the WE area, to accommodate the compensating reaction. The electrodes are placed at equal distance (∼1 cm) from each other, as shown schematically in Fig. 1a. This separation distance prevents interference between the compensating reaction species with the WE electrochemical reaction. The cell has a volume of 6 cm^3, in order to accommodate the size of the RE, and to facilitate calibration of the optical deflection sensing scheme. The electrodes are inserted at the top of the cell through openings of the same diameter. This helps to minimize the exposure to air and evaporation of the electrolyte solution. The front of the cell is fitted with a glass window to accommodate the optical beam deflection sensing scheme, and to provide direct visual access to the microcantilevers for control of their immersion depth into the electrolyte solution and alignment of the laser beams onto the apex of each microcantilever. Another glass window at the back of the cell, when removed, grants access to the back of the microcantilevers for calibration of the deflection measurements by interferometry [17].

2.2.2. Electrical contact to the WE

Electrical contacts to each electrode are made outside the cell so as to avoid the possibility of electrochemical reactions occurring at the contact points. In particular, due to its small size, special care was taken to protect the WE contact point from the electrolyte solution. The active (WE) and the reference microcantilever chips sit in grooves and are mechanically held with beryllium/copper clips (contact strips type H, Laird Technologies, USA) at the end of a Kel-F® rod attached to a micropositioner. The grooves are angled at 15° with respect to the front glass window of the cell. This angle is used to separate the reflected spot from the glass and the reflected spot from the microcantilever's apex impinging the position sensing photodetector (PSD), since the former can alter the deflection measurements [6] (Fig. 1a). The active (WE) and reference microcantilevers are vertically immersed into the electrolyte using the micropositioner (model 9064-Z, NewFocus, USA) so that only the microcantilevers and a small portion of their chip are in the solution. Electrical contact is made only to the active microcantilever (WE), on the gold-coated side, at the end of the chip located outside the electrolyte solution, with the beryllium/copper clip, as illustrated in Fig. 1b and Fig. 2. This technique offers a clean, easy and quick way to isolate the electrical contact point from the

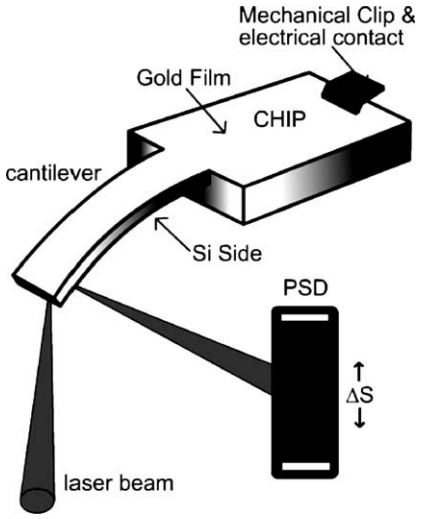

Fig. 2. Schematic representation of the optical beam deflection technique used to monitor the microcantilever deflection. The laser reflects off the apex of the Si side of the microcantilever and then hits the PSD. A gold film covers the other side of the microcantilever and the chip, rendering the surface conductive. Electrical contact is made to the gold-coated side at the opposite end of the chip.

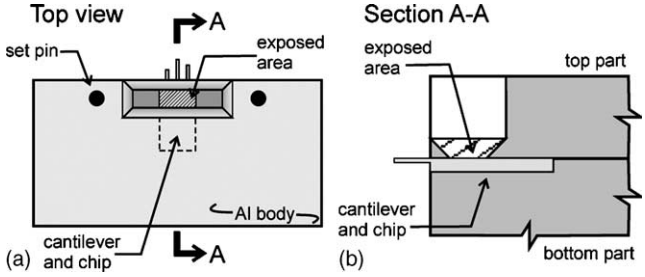

Fig. 3. Schematic representation of the aluminum fixture used for the application of Apiezon wax to the gold-coated microcantilever chip. An area of the chip is exposed to the wax. The set pins allow for the precise positioning of the Al body on top of the microcantilever chip for a reproducibly exposed area. (a) Top view of the assembly shows how the chip is held while exposing a fixed surface area of 1.0 mm^2 at 0.7 mm from the base of the microcantilevers. (b) Side view of the assembly.

electrolyte solution. It avoids the use of epoxy resin to encapsulate the electrical contact as employed by other groups [5–8,11], which may induce some level of contaminations in the electrochemical cell. No electrical contact is made to the reference microcantilever.

2.2.3. The microcantilever as an electrode

To perform electrochemical experiments, the surface of a silicon microcantilever was rendered electrically conductive by thermally evaporating a 100 nm film of Au on a 10 nm Ti adhesion layer. The resulting film has an average grain size of 100 ± 60 nm with a RMS roughness of 1.0 ± 0.2 nm, on a 1 μm length scale. X-ray diffraction revealed a strongly (1 1 1) textured Au film. The metal films were deposited on one side of the active microcantilever, as shown schematically in Fig. 2.

Rectangular silicon microcantilevers were chosen for the WE for two principal reasons. First, the rectangular shape makes for a simpler theoretical treatment [19] when converting the microcantilever deflection signal into a surface stress value. Secondly, the silicon surface of the microcantilever is reflective enough to allow the position-sensing laser light to reflect directly off it (opposite the metal-coated side where the potential is applied), as shown in Fig. 2. Hence, one does not need to reflect the laser light off the gold-coated side of the microcantilever, as is the case for silicon nitride microcantilevers used in AFM and in many of the reported microcantilever-based surface stress experiments. This allows us to avoid artefacts in the deflection measurement resulting from changes in surface reflectivity that occur when applying a potential to a gold surface. A large change in the reflectivity can be expected due to electrochemical reactions, such as hydrogen or oxygen adsorption [9], and can contribute to an artificial microcantilever response if the detected signal is not independent of the laser intensity. This can also be of particular concern when studying conducting polymer films that change color as a function of the applied potential.

In many cases, knowledge of the working electrode area (i.e. the area of the microcantilever and chip immersed in the electrolyte) is of significant importance as it enables one to quantify the current density (amount of charge consumed per unit area) during an electrochemical reaction. In particular, to obtain a reproducible thickness of an electrochemically deposited polymer film, it is important to control the surface area of the WE in contact with the electrolyte. Simply dipping the part of the microcantilever chip in the electrolyte solution makes it difficult to estimate the actual surface area in the solution due to the formation of a meniscus. A technique for delimiting the area of the WE in contact with the electrolyte was therefore implemented. The microcantilever chip was placed in an aluminium fixture, holding the chip securely in place while exposing an area on the microcantilever chip. This setup is shown schematically in Fig. 3. A layer of Apiezon wax W, is then deposited on the exposed area of the microcantilever chip. The masked region gives an electrode area of 1.0 mm^2. The precision on the measurement of the electrode area is hard to estimate and is mostly affected by the uncertainty in the adhesion between the wax and gold surface, at the masked region/gold surface boundary. The reproducibility of the electrochemically deposited PPy film thickness found to better than 3% (see Section 3.2.2) can give an appreciation for its value. The Apiezon wax is partly dissolved in trichloroethylene (TCE) to facilitate its application. The solvent is then left to evaporate, leaving the wax to harden for a few minutes, before using the microcantilever as an electrode. Other solvents such as chloroform and methanol were also tested but the best results were obtained with TCE. Heating the wax was found to be inadequate as it would cool down and harden before being deposited. Note that we did not encounter any contamination issues with the presence of the wax in aqueous solution.

2.2.4. The deflection sensing scheme

The differential microcantilever-based sensor is operated in a static mode, where the microcantilever deflections are monitored using an optical beam technique. A fiber-coupled laser diode (model # FMXL112-00, Bluesky Research, USA), operating at a wavelength of 635 nm, is used as a light source. The laser light is fed into two singlemode optical fibers by a 50/50 coupler. The light is then focused onto the apex of each microcantilever using commercial focusers (custom made by Brimrose, USA) having a working distance of 25 mm with a measured spot size of 24.6 μm (measured at the maximum intensity/e^2). The displacement of the reflected laser beams are monitored by two linear one-dimensional PSD (model 1L10, ON-TRAK Photonics, USA). Each PSD is located 24 mm away from the microcantilevers. The photocurrents generated at the PSD terminals by the impinging light spot are converted into voltages by home built precision transimpedance amplifiers [4]. The output voltage, V_{pos}, is directly proportional to the absolute position of the light spot on the PSD, $S = V_{pos}/2$. A 16-bit analog-to-digital converter from National Instruments, card model # PCI-6035E, digitizes the signal which is finally stored on a computer with a LabView program.

2.3. Calibration

For small deflections, the microcantilever deflection (Δz) is linearly proportional to the acquired PSD signal (ΔS):

$$\Delta z = C_{cal} \Delta S \tag{1}$$

For accurate quantitative surface stress measurements, the use of an interferometer, to simultaneously measure the cantilever deflection, is recommended to calibrate this relation [17]. The relation can alternatively be determined geometrically using the following approximate equation:

$$\Delta z \cong \frac{l}{2L} \Delta S \tag{2}$$

where l is the microcantilever effective length and L the distance between the microcantilever and the PSD. The microcantilever effective length is defined as the length at which the laser beam hits the microcantilever. For our particular system geometry, a 6% percentage difference is found between the interferometer calibration constant and the geometrical calibration constant. A value of $C_{cal} = (6.8 \pm 0.3) \times 10^{-3}$ is found, for the system described herein. The major source of error in C_{cal} comes from the uncertainty in the measurements of the distance L. However, in our experimental setup, L is fixed for all measurements, so that random errors in the experiments are associated with the determination of the effective length of the microcantilever, l. A systematic error is also introduced from the fact that the calibration is done in air whereas experiments are performed in liquids. This slightly modifies the path length of the reflected laser beam, L. However, we found that this effect changes L, and thus C_{cal}, by a negligible amount.

The surface stress ($\Delta\sigma$) is in turn directly proportional to the microcantilever deflection (Δz) through [17]:

$$\Delta\sigma = \frac{4}{3(1-\upsilon)} \frac{l}{wt} k_{rect} \Delta z \tag{3}$$

where υ, l, w, t and k_{rect} are Poisson's ratio, the length, width, thickness and spring constant the microcantilever, respectively. The 4/3 factor takes into account the difference in the cantilever beam curvature resulting from a uniform surface stress, as opposed to a concentrated load applied at the tip. The microcantilever geometrical properties are all measurable parameters. A high resolution SEM was used to accurately determine each dimension to improve on the accuracy of the surface stress measurements. Poisson's ratio is taken to be 0.064 [18], because the single crystal Si microcantilever surface is in the $\{1\,0\,0\}$ plane and the microcantilever edges are along the $\langle 1\,1\,0\rangle$ direction. The spring constant was obtained using Sader's method [19], which simply requires the measurements of the microcantilever length, width, and its fundamental resonant frequency and corresponding quality factor. An FFT network analyzer (model SR770, Stanford Research, USA) was used to acquire the power spectrum density of the microcantilever deflection signal. The consequences of the microcantilever gold coating ($t_{Au} = 100$ nm) on the mechanical properties of the microcantilever beam are taken into account by the measurements of the microcantilever beam thickness and of its spring constant. Its effect on Poisson's ratio is assumed negligible in this case. By carefully determining the value of each parameter in Eq. (3) we can measure surface stress values with an accuracy of 10%. The precision with which the spring constant, k_{rect}, and the thickness, t, can be measured are the major contributions of error in surface stress measurements, followed by the uncertainty in L. The advantages of using Eq. (3) over Stoney's formula is that it is not necessary to know the Young's modulus, E, of the microcantilever structure.

Our device can achieve a deflection sensitivity of 0.2 nm, in a 3 Hz bandwidth, by performing time-averaging on the acquired deflection signal, resulting in an ultimate surface stress sensitivity of 1×10^{-4} N/m. The surface stress sensitivity was calculated for the specific microcantilevers used here but can be improved with a lower spring constant (longer, thinner and narrower microcantilevers). The maximum detectable deflection signal of our PSD corresponds to a surface stress of 50 N/m, providing us with a dynamic range of 5×10^5. The maximum surface stress value was calculated for the specific geometry of the experimental setup and is limited by the finite size of the PSD. In fact, as described by Eq. (2), the dynamic range can be lowered or amplified by, respectively, increasing or reducing L, at the cost of inversely affecting the sensitivity of the instrument.

Eq. (3) refers to a relative change in surface stress between both sides of the microcantilever. Therefore, for this microcantilever-based sensor technique to work, one side of the microcantilever must remain inert and non-reactive throughout the experiment. In such a case, the studied

phenomenon only occurs on one side of the microcantilever and changes in surface stress measurements are obtained. Otherwise, competing reactions from both sides of the microcantilever may lead to results that are difficult, if not impossible, to interpret. Methods for passivating the backside of microcantilevers often present a difficult challenge and are the subject of ongoing research [20].

To perform accurate differential microcantilever-based sensor measurements, both active and reference microcantilever deflection signals should be converted into surface stress before the signals are subtracted. Indeed many parameters affect the magnitude of the deflection signals. Overall, in the system described herein, since both microcantilever-based sensors have almost identical L, it is the difference in spring constants between the active and reference microcantilevers that mainly affects the difference in magnitude of the deflection signals. It is therefore imperative to measure the spring constant of both active and reference microcantilevers independently, and transform the active and reference microcantilever deflection signals into surface stress to obtain a proper differential signal.

3. Results and discussion

3.1. The differential mode

The high sensitivity of the microcantilever-based surface stress sensors makes them extremely responsive to physical and chemical stimuli. For example, during an experiment, an *active* microcantilever will deflect as a result of the electrochemical reaction occurring on its surface, but it will also deflect due to other factors. These *parasitic* microcantilever deflections occur as a result of several effects, such as temperature changes (bimetallic effect), turbulent flow around the microcantilever, environmental noise, or uncontrolled chemical reactions on the back side (opposite the sensing surface) of the microcantilever. It is therefore imperative that such deflections be removed from the final measurements if the surface stress data are to be analyzed correctly. A *reference* microcantilever can be tailored to only be reactive to these parasitic stimuli and serve as an effective reference sensor. A subtraction of a reference signal from an active microcantilever signal will give a measurement of surface stress that is purely due to the electrochemical reaction in question [21–23].

In order to illustrate the effectiveness of the differential microcantilever-based sensor, an experiment was conducted in which both the reference and active microcantilever deflections were simultaneously monitored. Electrochemical cycling between 0 and 700 mV (versus Ag/AgCl) of the gold-coated surface of the active microcantilever, in a 0.1 M perchloric acid solution ($HClO_4$) was performed. While the electrochemical reaction is carried out on the active microcantilever (WE), the electrolyte solution temperature is varied, with the use of a thermoelectric element (TE technology, USA) in contact with the back of the cell. For the purpose of subtracting thermal fluctuations and/or environmental noises (such as mechanical vibrations) from the active microcantilever (WE) signal, the reference microcantilever is identically covered with a Ti and Au film to make it equally sensitive to temperature variations through the bimetallic effect. No electrical contact is made to the reference microcantilever.

3.1.1. Differential surface stress at the solid–liquid interface

Electrochemical cycling between 0 and 700 mV (versus Ag/AgCl), in a 0.1 M perchloric acid solution ($HClO_4$), causes adsorption of ClO_4^- anions on the gold-coated surface of the active microcantilever. In turn, the anion adsorption induces a change of surface stress on the active microcantilever (WE). A compressive surface stress of -1.28 ± 0.13 N/m is measured when the WE potential is changed from 0 to 700 mV, in agreement with previously reported value by Ibach et al. [14]. Within this potential window the Au(1 1 1) surface stays in an unreconstructed state and the surface stress measured is entirely due to specific adsorption of ClO_4^- ions [14].

Fig. 4a shows the active microcantilever (WE) signal during five cycles of ClO_4^- anion adsorptions on gold along with

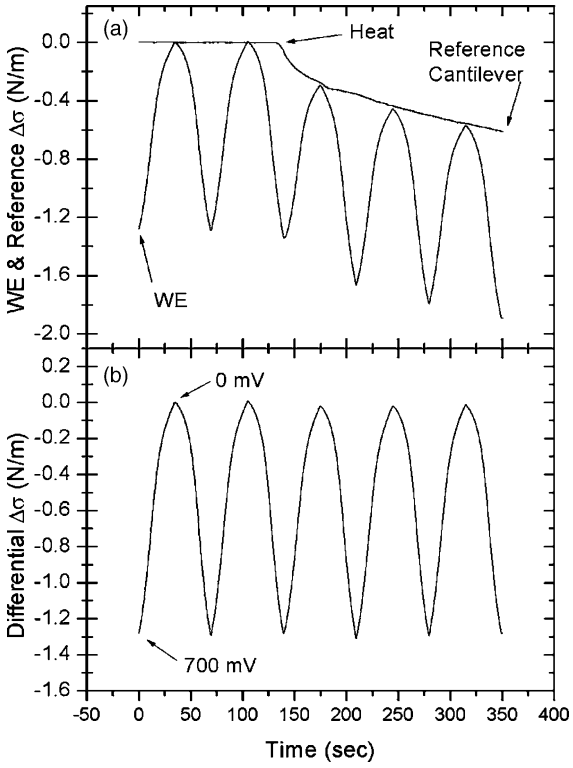

Fig. 4. (a) Active microcantilever (WE) signal during five cycles between 0 and 700 mV, and reference microcantilever signal. At $t = 130$ s heat is induced and the reference microcantilever starts to drift. In the active microcantilever (WE) signal, signs of bending due to the bimetallic effect are also present. (b) The reference microcantilever signal is subtracted from the active microcantilever signal. The resulting differential signal shows no apparent sign of temperature variations.

the reference microcantilever signal. Because no potential is applied to the reference microcantilever, no adsorption and no potential-induced surface stress takes place. At $t = 130$ s, the thermoelectric element starts to heat the electrolyte solution, as shown by the onset of the reference microcantilever deflection. While the electrochemical reaction continues on the active microcantilever (WE) surface, sign of bending due to the bimetallic effect are also present. Fig. 4b shows the differential microcantilever signal, where the reference microcantilever surface stress signal is subtracted from the active microcantilever (WE) surface stress signal. It is clear from Fig. 4b that the reference microcantilever acts like an effective reference sensor, and that temperature fluctuations can be properly eliminated (on the scale of the active microcantilever signal) from the active microcantilever (WE) signal.

3.2. A polypyrrole microactuator

Our instrument was used to study the actuation properties of a conducting polymer, polypyrrole (PPy). PPy swells when electrochemically switched from its oxidized to reduced state, thus making it a potential candidate as an artificial muscle [24]. In order for this material to be used as a conventional microactuator, it is important to characterize its properties, particularly potential-induced surface stress changes as a function of the film growth mode, thickness, number doping/dedoping cycles, etc.

3.2.1. Electrochemical signal

To demonstrate that electrochemical processes occurring on the microcantilever surface can be effectively detected, cyclic voltammetry (CV) is performed on the WE gold surface with the $Fe(CN)_6^{3-/4-}$ redox couple. A peak separation of 71 mV (versus Ag/AgCl) is observed (Fig. 5). This value is acceptable compared to the theoretical peak separation of 59 mV expected for a single electron transfer reaction. The discrepancy is probably due to the contact resistance. In addition the intensities of the cathodic and anodic peak are equal which is indicative of a reversible process.

3.2.2. Electrochemical deposition of PPy

The PPy film is electropolymerized from an aqueous solution containing 0.1 M Py and 0.1 M NaDBS at a constant potential of +550 mV (versus Ag/AgCl). This value of the potential is chosen to ensure a more uniform film thickness [25]. The time for which this potential is applied determines the thickness of the PPy film deposited on the microcantilever. Indeed, because the deposition rate of the PPy film is constant (steady-state value of the polymerization current), the PPy film thickness depends linearly on time.

For the data presented here, the potential was applied for 200 s. To verify the reproducibility of the PPy film thickness obtained on the 1.0 mm^2 WE, direct AFM imaging of steps made to the PPy film, by scratching the surface with a razor blade, was performed. AFM measurements were done on freshly polymerized PPy film (oxidized state). Prior to

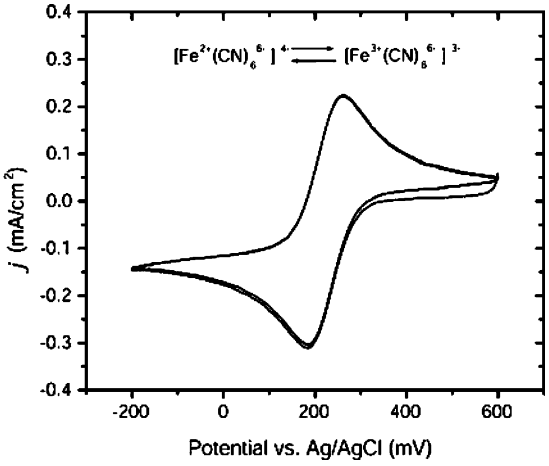

Fig. 5. Cyclic voltammograms of a microcantilever's bare gold surface in an aqueous solution of 2 mM $K_3Fe(CN)_6$ and 0.2 M KCl electrolyte. The one electron reduction and oxidation of $Fe(CN)_6^{3-/4-}$ at the gold surface results in a cathodic peak at 187 mV and an anodic peak at 258 mV. The peak separation of 71 mV (which is close to the theoretical value of 59 mV), and equal cathodic and anodic peak current intensities are consistent with a reversible redox process.

imaging, the AFM was calibrated in the vertical direction by a grid sample with fixed depth. Fig. 6 shows the AFM thickness results. Imaging was done in both contact and tapping mode to investigate the effect of tip loading in the height analysis. No significant step height differences were revealed

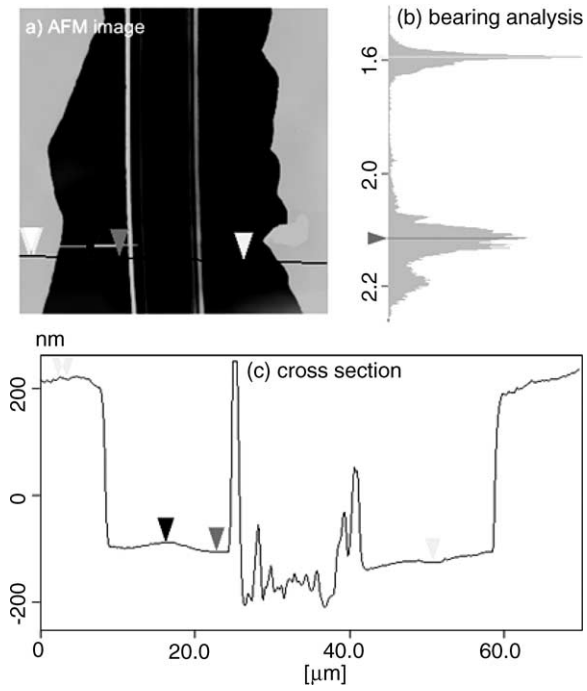

Fig. 6. (a) AFM contact mode image of a step, made by scratching the PPy film with a razor blade, to determine its thickness. The light and the dark grey regions are the PPy film and the gold substrate, respectively. The image size is 70 μm × 70 μm, and height scale is 500 nm. (b) Bearing analysis and (c) cross section analysis, to measure the height difference between the polymer and the gold surface.

by comparing the two imaging modes. In addition, following a simple Hertz model, the possible indentations produced by the tip are only on the order of the a few nm. The bearing analysis of the NanoscopeIII software (version.4.43r8, Veecoo instruments, USA) was used to measure the height difference between the PPy film and the gold substrate. The bearing analysis gives a statistical distribution of the different heights in the image. The width of the height distribution in the bearing analysis is used to estimate the precision of a measurement. The average value obtained for a series of PPy films on microcantilevers gives a consistent PPy film thickness of 304 nm with a standard deviation of 9 nm. This result shows the consistency of the implemented method for defining the WE area, with a reproducibility of 3% in the PPy film thickness. In addition, the interference color of PPy(DBS) on gold, green, matches the expected reported color for that thickness [25] which confirms the accuracy of the measured film thickness. The reproducibility of the PPy film thickness is mostly affected by the variability of the polymerization current, and by the error of the AFM measurements. In fact, the non-uniformity of the PPy film, although minimized, increases the error in the AFM measurements [25].

3.2.3. *Electrochemical actuation of PPy*

The PPy film is then actuated by cyclic voltammetry in a 0.1 M Na(DBS) solution while monitoring the active microcantilever deflection. The electrode potential is initially swept from its rest potential to −850 mV, and back to +300 mV at a scan rate of 100 mV/s. Within this potential window, the PPy film is cycled between its oxidized and reduced states:

$$\underset{\text{oxidized}}{PPy^{+}(DBS^{-})} \overset{e^{-}+Na^{+}}{\underset{-e^{-}-Na^{+}}{\rightleftharpoons}} \underset{\text{reduced(swelled)}}{PPy^{0}(DBS^{-}Na^{+})} \quad (4)$$

The reduced state is characterized by a swelling of the polymer matrix causing a bending of the microcantilever beam. Fig. 7a and b shows the current and surface stress changes for a PPy-coated microcantilever during three doping/dedoping cycles. Maximum microcantilever deflections are achieved when going from the anodic (oxidation) to the cathodic (reduction) peak potentials. A maximum surface stress change of 2.88 ± 0.29 N/m is obtained for the studied PPy(DBS) film in 0.1 M NaDBS under the specific PPy polymerization conditions used here. The PSD sum signal (i.e. laser intensity) is shown in Fig. 7c. The very small intensity variations observed (on the order of a few mV) clearly indicate that no polymer is present on the back side of the microcantilever. As we have observed in other experiments, when reflecting the laser beam off the PPy side of the microcantilever, due to the change in colors, variations as large as a few volts are detected when the polymer is switched from its oxidized to reduced state. As demonstrated in Fig. 7, surface stress changes induced by electrochemical reactions can be measured using the microcantilever sensor described in this paper.

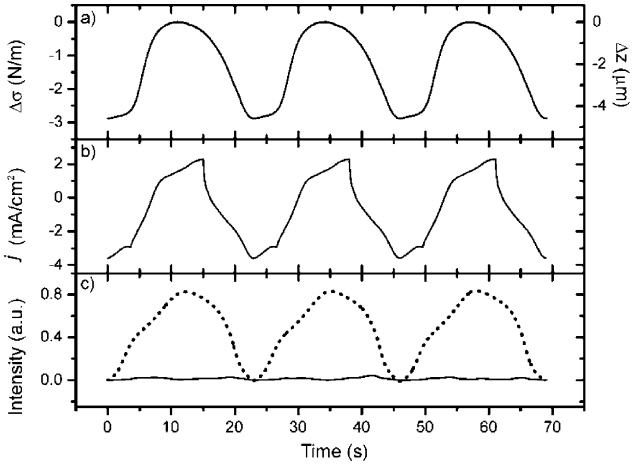

Fig. 7. (a) Surface stress and (b) current vs. time plots measured simultaneously during cyclic voltammetric scans of PPy-coated microcantilevers in 0.1 M Na(DBS) solution. The potential is swept at 100 mV/s between −850 and +300 mV. The data presented has been chosen to start at the cathodic peak, but the experiment is initially started from the rest potential. For each cycle, the maximum change in deflection is observed at the anodic (at 7, 32 and 54 s) and cathodic (at 0, 23 and 46 s) peaks. Panel (c) shows the variations in the reflected laser intensity off the microcantilever Si back side (solid line) and of the Au-coated side (dotted line, measured separately) as a function of time. These data indicate that the PPy film is present only on the Au-coated side, since variations in the reflected light intensity are not observed on the Si side when the polymer is switched from an oxidized to a reduced state.

4. Conclusion

We have outlined many potential parameters which can influence the microcantilever sensor response during electrochemical reactions. In order to circumvent these adverse effects we have presented an instrument capable of measuring microcantilever deflections while isolating sensitive surface stress changes induced only by those of specific electrochemical reactions. A method defining the WE area to a 1 mm^2 surface was developed. It allowed a quantitative measure of the current density and for 3% reproducibility in the thickness of electrochemically deposited PPy films. The effectiveness of the reference microcantilever sensor was verified by varying the electrolyte temperature while anion adsorption was performed on the active microcantilever. The resulting differential signal showed no measurable sign of temperature fluctuations.

We measured a potential-induced change in surface stress, at the solid (Au(1 1 1))–liquid ($HClO_4$ electrolyte) interface, of −1.28 N/m when cycled between 0 and 700 mV (versus Ag/AgCl), in 0.1 M $HClO_4$ electrolyte solution. In addition, the surface stress induced by electromechanical transformations in a PPy thin film was measured. The ion doping/dedoping of a dodecyl benzenesulfonate-doped polypyrrole (PPy(DBS)) film in an aqueous solution of Na(DBS), generated a compressive surface stress of −2.88 N/m when switched between its oxidized and reduced states. We are currently conducting an in-depth study of these systems to

understand the mechanism behind the sensor's response and the origin of the measured surface stress. The instrument presented herein can be a useful and promising tool to characterize and optimize, on the micrometer scale, the mechanical properties of electroactive polymer films [26].

Acknowledgments

This work was supported by the Natural Science and Engineering Research Council of Canada (NSERC). Both V.T.-C. and M.G. would like to acknowledge the financial support given by McGill University through its McGill Major Fellowships program. M.G. would like to thank Le Fonds Québécois de la Recherche sur la Nature et les Technologies (FQRNT) for financial support (Doctoral Fellowship). L.Y.B. thanks NSERC for financial support through a postdoctoral fellowship. The authors would also like to thank, Antonella Badia and R.B. Lennox for many helpful discussions, Benjamin Smith and Manuel Pumarol for their help in AFM imaging, Robert Gagnon for the X-ray measurements and SEM imaging and Eddie Del Campo for machining the cell.

References

[1] H.P. Lang, M. Hegner, Ch. Gerber, Nanotechnology 13 (2002) 29–36.
[2] R. Berger, Ch. Gerber, H.P. Lang, J.K. Gimzewski, Microelectr. Eng. 35 (1997) 373–379.
[3] R. Raiteri, M. Grattarola, H.-J. Butt, P. Skladal, Sens. Actuators B 79 (2001) 115–126.
[4] M. Godin, O. Laroche, V. Tabard-Cossa, L.Y. Beaulieu, P.J. Williams, P. Grutter, Rev. Sci. Instrum. 74 (2003) 4902.
[5] T.A. Brunt, T. Rayment, S.J. O'Shea, M.E. Welland, Langmuir 12 (1996) 5942–5946.
[6] T.A. Brunt, E.D. Chabala, T. Rayment, S.J. O'Shea, M.E. Welland, J. Chem. Soc., Faraday Trans. 92 (1996) 3807.
[7] S.J. O'Shea, M.E. Welland, T.A. Brunt, A.R. Ramadan, T. Rayment, J. Vac. Sci. Technol. B 14 (1996) 1383–1385.
[8] R. Raiteri, H.-J. Butt, J. Phys. Chem. 99 (1995) 15728–15732.
[9] T. Miyatani, M. Fujihira, J. Appl. Phys. 81 (1997) 7099–7115.
[10] T. Miyatani, Fujihira F M., Jpn. J. Appl. Phys., Part 1 36 (1997) 5280–5281.
[11] M. Lahav, C. Durkan, R. Gabai, E. Katz, I. Willner, M.E. Welland, Angew. Chem. Int. Ed. 40 (2001) 4095–4097.
[12] M. Roemer, T. Kurzenknabe, E. Oesterschulze, N. Nicoloso, Anal. Bioanal. Chem. 373 (2002) 754–757.
[13] F. Quist, V. Tabard-Cossa, A. Badia, J. Phys. Chem. B 107 (2003) 10691–10695.
[14] H. Ibach, C.E. Bach, M. Giesen, A. Grossmann, Surf. Sci. 375 (1997) 107–119.
[15] W. Haiss, R.J. Nichols, J.K. Sass, K.P. Charle, J. Electroanal. Chem. 452 (1998) 199–202.
[16] M. Godin, P.J. Williams, V. Tabard-Cossa, O. Laroche, L.Y. Beaulieu, R.B. Lennox, P. Grutter, Langmuir 20 (2004) 7090–7096.
[17] M. Godin, V. Tabard-Cossa, P. Williams, P. Grutter, Appl. Phys. Lett. 123 (2002) 1223.
[18] W.A. Brantley, J. Appl. Phys. 44 (1973) 534–535.
[19] J.E. Sader, J.W.M. Chon, P. Mulvaney, Rev. Sci. Instrum. 70 (1999) 3967–3969.
[20] R. Raiteri, H.-J. Butt, M. Grattarola, Electrochem. Acta 46 (2000) 157–163.
[21] H.P. Lang, R. Berger, F. Battiston, J.-P. Ramseyer, E. Meyer, C. Andreoli, J. Brugger, P. Vettiger, M. Despont, T. Mezzacasa, L. Scandella, H.-J. Guntherodt, C. Gerber, J.K. Gimzewski, Appl. Phys. A: Solids Surf. 66 (1998) S61–S64.
[22] J. Fritz, M.K. Baller, H.P. Lang, H. Rothuizen, P. Vettiger, E. Meyer, H.-J. Guntherodt, Ch. Gerber, J.K. Gimzewski, Science 288 (2000) 316–318.
[23] H. Jensenius, J. Thaysen, A.A. Rasmussen, L.H. Veje, O. Hansen, A. Boisen, Appl. Phys. Lett. 76 (2000) 2615–2617.
[24] E.W.H. Jager, O. Inganas, I. Lundstrom, Science 288 (2000) 2335–2338.
[25] E. Smela, J. Micromech. Microeng. 9 (1999) 1–18.
[26] Y. Bar-Cohen, S. Sherrit, S.-S. Lih, Smart materials and structures, Proc. SPIE 4329 (2001) 319–327.